JOURNAL OF GEOPHYSICAL RESEARCH, VOL. 114, D05304, doi:10.1029/2008JD010993, 2009

Analysis of the summertime buildup of tropospheric ozone abundances over the Middle East and North Africa as observed by the Tropospheric Emission Spectrometer instrument

Jane J. Liu,[1] Dylan B. A. Jones,[1] John R. Worden,[2] David Noone,[3] Mark Parrington,[1] and Jay Kar[1]

Received 15 August 2008; revised 11 December 2008; accepted 31 December 2008; published 7 March 2009.

[1] We use the GEOS-Chem chemical transport model to interpret observations of tropospheric ozone from the Tropospheric Emission Spectrometer (TES) satellite instrument in summer 2005. Observations from TES reveal elevated ozone in the middle troposphere (500–400 hPa) across North Africa and the Middle East. Observed ozone abundances in the middle troposphere are at a maximum in summer and a minimum in winter, consistent with the previously predicted summertime "Middle East ozone maximum." This summertime enhancement in ozone is associated with the Arabian and Sahara anticyclones, centered over the Zagros and Atlas Mountains, respectively. These anticyclones isolate the middle troposphere over northeast Africa and the Middle East, with westerlies to the north and easterlies to the south, facilitating the buildup of ozone. Over the Middle East, we find that in situ production and transport from Asia provides comparable contributions of 30–35% to the ozone buildup. Over North Africa, in situ production is dominant (at about 20%), with transport from Asia, North America, and equatorial Africa each contributing about 10–15% to the total ozone. We find that although the eastern Mediterranean is characterized by strong descent in the middle and upper troposphere in summer, transport from the boundary layer accounts for about 25% of the local Middle Eastern contribution to the ozone enhancement in the middle troposphere. This upward transport of boundary layer air is associated with orographic lifting along the Zagros Mountains in Iran and the Asir and Hijaz Mountain ranges in Saudi Arabia, and is consistent with TES observations of deuterated water.

Citation: Liu, J. J., D. B. A. Jones, J. R. Worden, D. Noone, M. Parrington, and J. Kar (2009), Analysis of the summertime buildup of tropospheric ozone abundances over the Middle East and North Africa as observed by the Tropospheric Emission Spectrometer instrument, *J. Geophys. Res.*, *114*, D05304, doi:10.1029/2008JD010993.

1. Introduction

[2] Tropospheric ozone (O_3) is a major atmospheric pollutant and a greenhouse gas. It also plays an important role in determining the oxidative capacity of the atmosphere because it is a key precursor of the hydroxyl radical (OH), the dominant atmospheric oxidant. The distribution of tropospheric ozone reflects a balance between in situ photochemical sources and sinks, and atmospheric transport of ozone and its precursors. It is now recognized that long-range transport of pollution can have a significant impact on regional budgets of tropospheric ozone. There have been numerous studies based on model simulations, and aircraft and surface observations which have examined the intercontinental transport of ozone between North America, Europe, and Asia [e.g., *Berntsen et al.*, 1999; *Yienger et al.*, 2000; *Wild and Akimoto*, 2001; *Fiore et al.*, 2002; *Lelieveld et al.*, 2002; *Li et al.*, 2002; *Lawrence*, 2004; *Duncan and Bey*, 2004]. Studies have also examined the influence of transport on the ozone distribution in the Middle East [*Li et al.*, 2001] and the Mediterranean region [*Lelieveld et al.*, 2002; *Duncan et al.*, 2008].

[3] The ozone distribution in the vicinity of the Middle East and North Africa in summer is of particular interest because in the upper troposphere the region is strongly influenced by transport of Asian pollution associated with the extended Asian monsoon anticyclone system [*Lawrence*, 2004]. Previous studies [e.g., *Park et al.*, 2004; *Li et al.*, 2005; *Randel and Park*, 2006] have shown that this anticyclone has a significant impact on the distribution of trace gases in the upper troposphere and lower stratosphere (UTLS). The influence of Asian pollution has also been observed in the middle troposphere in the eastern Mediterranean [*Lelieveld et al.*, 2002]. Furthermore, European pollution is transported into the region at low altitudes in summer [*Duncan and Bey*, 2004; *Duncan et al.*, 2008]. As a

[1]Department of Physics, University of Toronto, Toronto, Ontario, Canada.
[2]Earth and Space Sciences Division, Jet Propulsion Laboratory, California Institute of Technology, Pasadena, California, USA.
[3]Department of Atmospheric and Oceanic Sciences, University of Colorado at Boulder, Boulder, Colorado, USA.

0148-0227/09/2008JD010993$09.00

result of the combined influence of Asian and European pollution, high levels of ozone precursors such as HCHO, CH_3COCH_3, and CH_3OH have been observed at all levels of the troposphere over the Mediterranean [*Lelieveld et al.*, 2002]. This has important implications for both air quality and climate in the region.

[4] In a previous modeling study, *Li et al.* [2001] suggested the existence of a seasonal buildup of tropospheric ozone in the middle troposphere over the Middle East. They suggested that this maximum is linked to the anticyclones and the large-scale subsidence in the middle and upper troposphere in this region. They emphasized the need for more observational evidence, especially from satellites, to confirm the presence of the ozone maximum. *Kar et al.* [2002] showed that climatological observations from SAGE II revealed elevated abundances of ozone over the Middle East in summer. However, this ozone maximum was not found in retrieved ozone column abundances from measurement by the Global Ozone Monitoring Experiment (GOME) [*Liu et al.* 2006] or using the residual method based on ozone data from other satellite instruments [*Fishman et al.*, 2003; *Ziemke et al.*, 2006]. The Tropospheric Emission Spectrometer (TES) is providing continuous global measurements of the vertical distribution of tropospheric ozone, and thus offers new information to enhance our understanding of the ozone maximum in the Middle East. Recently, J. Worden et al. (Tropospheric ozone and the Asian monsoon, submitted to *Journal of Geophysical Research*, 2009) examined the vertical distribution of ozone observed by TES over the Middle East and South Asia and showed that the ozone distribution over the Middle East is stratified with high abundances of ozone of nearly 100 ppbv in the middle troposphere in summer.

[5] In this paper, we examine the mechanisms contributing to the summertime ozone buildup over the Middle East in the context of the new observations from TES. We use the GEOS-Chem global chemical transport model (CTM) to better understand the processes responsible for the high concentrations of ozone observed by TES across North Africa and the Middle East. We first present, in section 2, a brief discussion of the TES instrument and the GEOS-Chem model and summarize the ozone enhancement observed by TES over the Middle East and surrounding areas. In section 3 we discuss the summertime meteorological conditions in the Middle East. In section 4 we present the GEOS-Chem simulation of the distribution of O_3, H_2O, and CO and discuss the mechanism responsible for the ozone enhancement. We then examine in section 5 the ozone photochemical production in the region and quantify the contribution of in situ chemical production and long-range transport of ozone to the ozone enhancement. In section 6 we examine TES observations of H_2O and HDO/H_2O to assess the consistency of the model simulation with the constraints provided by the TES data on the transport pathways over North Africa and the Middle East. Finally, in section 7 we summarize our results.

2. Data and Model

2.1. TES

[6] The TES instrument [*Beer et al.*, 2001] is a nadir viewing Fourier transform spectrometer that was launched on the NASA EOS Aura spacecraft on 15 July 2004. The Aura satellite is in a Sun-synchronous orbit at an altitude of 705 km with an inclination of 98.2° and orbit repeat cycle of 16 days. The instrument measures thermal emission between 3.3 and 15.4 μm and operates in a global survey mode, in which the observations are spaced about 2° along the orbit track, and in a step-and-stare mode, in which the observation are made every 40 km along the orbit. The footprint of the measurement on the ground at the nadir view is 8 × 5 km. A detailed discussion of the TES retrievals of ozone is given by *Bowman et al.* [2006]. The retrievals have between 1 and 1.5 independent pieces of information (also referred to as degrees of freedom for signal (DOFS)) in the profile at midlatitudes in summer, with peak sensitivities in the lower and upper troposphere near 700 hPa and 300–400 hPa, respectively [*Parrington et al.*, 2008]. We use version V002 of the TES data, which were validated by *Nassar et al.* [2008] using ozonesonde measurements. They reported a positive bias of 3–11 ppbv in the upper troposphere and 4–9 ppbv in the lower troposphere. However, there is only one station (Isfahan) with two unflagged profiles from October 2004 to October 2006 over the Middle East and North Africa so that no definitive comparison could be made in their work between TES data and the ozonesonde profiles for this region (Ray Nassar, personal communication, 2008).

[7] TES also provides profile retrievals of water vapor (H_2O) and deuterated water vapor (HDO/H_2O) in the troposphere [*Beer et al.*, 2001]. *Shephard et al.* [2008] compared H_2O measurements from TES with nighttime radiosondes data from the National Centers for Environmental Prediction (NCEP). They found that the mean difference between the two data sets is less than 5% in the lower troposphere (at pressures greater than 600 hPa), increasing to a maximum of ~15% in the upper troposphere (300–200 hPa), with the radiosonde data being drier. *Worden et al.* [2006] characterized the error of the HDO/H_2O ratio and reported a precision of 1–2% in the ratio and a possible bias of 5% due to the HDO spectroscopic line strengths. The TES retrieval of the HDO/H_2O ratio is most sensitive near 700 hPa and has the least uncertainty in the tropics and highest uncertainty at higher latitudes.

2.2. GEOS-Chem Model

[8] The GEOS-Chem model [*Bey et al.*, 2001] is a global three-dimensional CTM driven by assimilated meteorological observations from the NASA Goddard Earth Observing System (GEOS-4) from the Global Modeling and data Assimilation Office (GMAO). We use version v7-02-04 of GEOS-Chem (http://www-as.harvard.edu/chemistry/trop/geos), with the resolution of the meteorological fields of 4° latitude × 5° longitude, degraded from their native resolution of 1° × 1.25°. The model includes a detailed description of tropospheric O_3-NO_x-hydrocarbon chemistry, including the radiative and heterogeneous effects of aerosols. We use a linearized ozone (Linoz) parameterization scheme based on work by *McLinden et al.* [2000] to represent the ozone in the stratosphere. Since assimilated meteorological fields produce excessive stratosphere-to-troposphere exchange [e.g., *Weaver et al.*, 1993; *Tan et al.*, 2004], we use a version of GEOS-Chem with a specified ozone flux boundary condition at the tropopause (Synoz) [*McLinden et al.*, 2000] for our tagged ozone analysis to

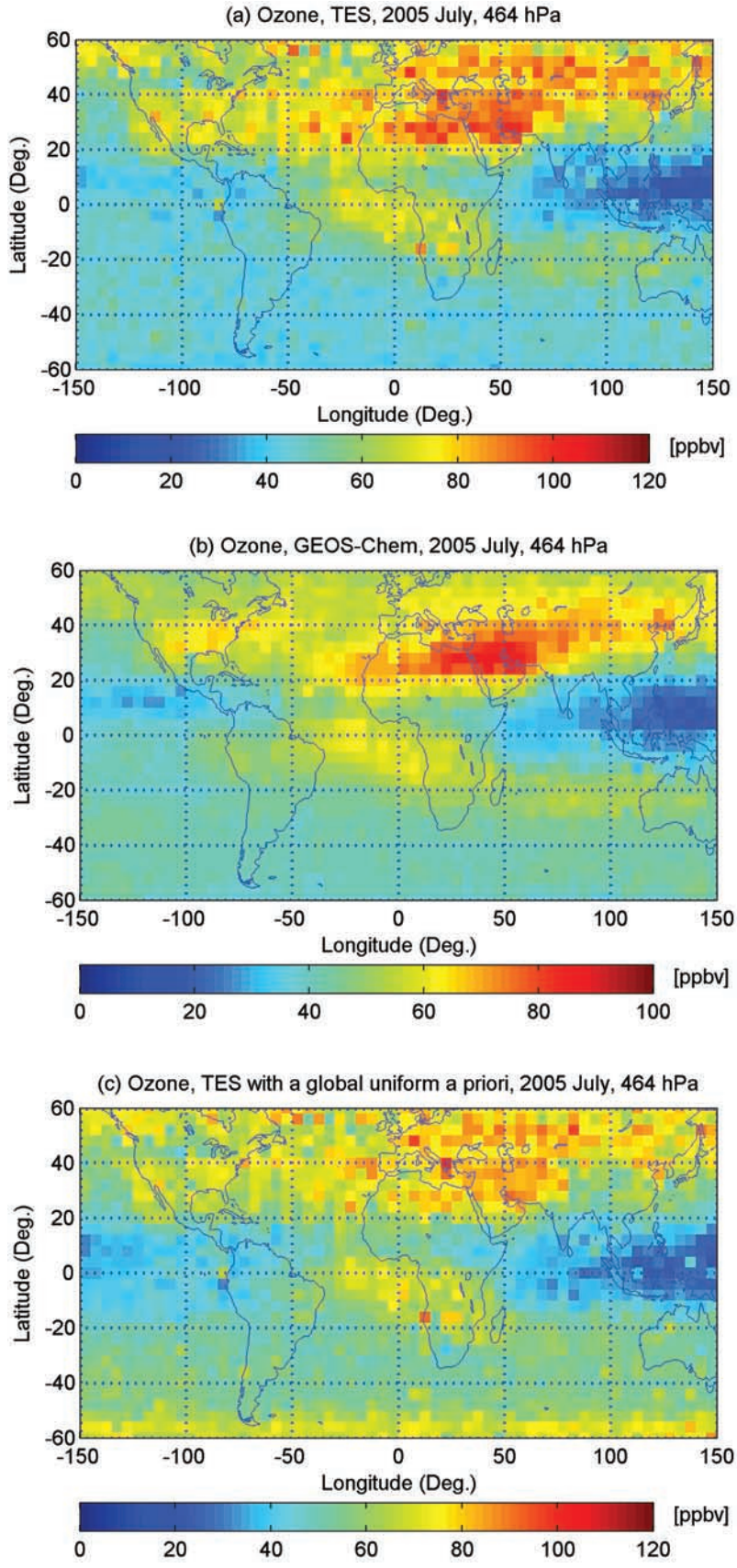

Figure 1. Monthly mean ozone mixing ratio in July 2005 at 464 hPa from (a) TES, (b) GEOS-Chem, smoothed with the local TES averaging kernels (see equation (1)), and (c) TES with a global uniform a priori. Note the maximum scale is 120 ppbv for TES data and 100 ppbv for GEOS-Chem data.

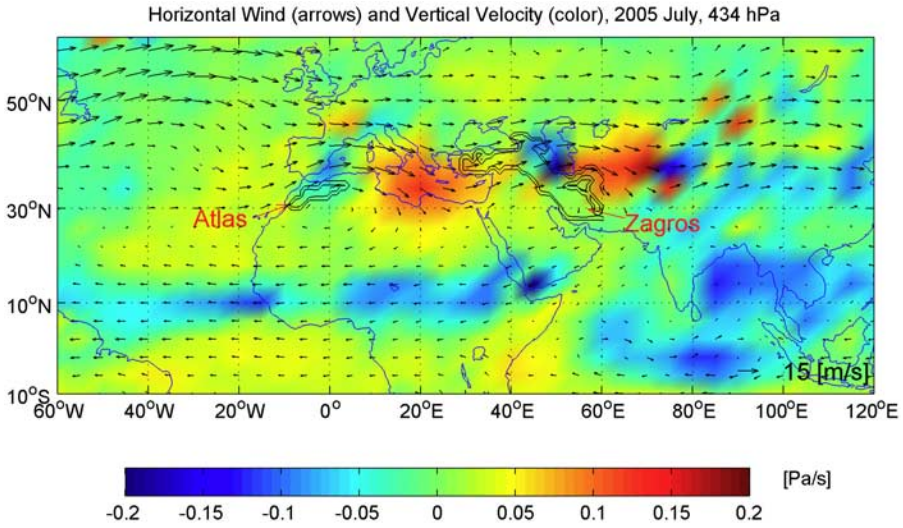

Figure 2. Horizontal wind vectors (arrows) overlaid with vertical velocity (dp/dt, Pa s^{-1}) for July 2005 at 434 hPa (~6.7 km) in GEOS-Chem (GEOS-4 fields). Red color indicates descent, while blue shows ascent. The double black lines delineate the Atlas and Zagros Mountains.

ensure that we do not overestimate the source of ozone from the stratosphere. We note that although the Synoz scheme correctly reproduces the annual global source of stratospheric ozone, it may not correctly capture the variability in the magnitude of the stratospheric ozone fluxes locally. We find, however, that over the Middle East during summer 2005, the period of our analysis, the mean differences in ozone abundances in the middle troposphere simulated with the Linoz and Synoz schemes are less than 3%.

[9] Several studies have evaluated the model simulation of tropospheric ozone in general and in the context of quantifying the impact of long-range transport of pollution on the distribution of tropospheric ozone [e.g., *Bey et al.*, 2001; *Martin et al.*, 2002; *Jaeglé et al.*, 2003; *Li et al.*, 2005; *Zhang et al.*, 2006]. Recently, *Parrington et al.* [2008] assimilated TES data into the GEOS-Chem model to better quantify the distribution of ozone over North America in summer 2006. In the version of the model employed here is based on work by *Parrington et al.* [2008], in which anthropogenic emissions are from the Global Emissions Inventory Activity (GEIA) [*Benkovitz et al.*, 1996], with emissions in the United States based on the Environmental Protection Agency (EPA) National Emission Inventory 1999 (NEI99) [*Hudman et al.*, 2007]. Emissions from biofuel combustion and biomass burning are from *Yevich and Logan* [2003] and *Duncan et al.* [2003], respectively. Global NO_x emissions from lightning are specified at 4.7 Tg N a^{-1}, on the basis of the parameterization of *Price and Rind* [1992] and with the vertical distribution of the NO_x emissions imposed according to *Pickering et al.* [1998].

2.3. Comparison of Modeled Ozone With TES Observations

[10] The monthly mean ozone mixing ratio retrieved from the TES instrument at 464 hPa in July 2005 is shown in Figure 1a. Enhanced ozone abundance is observed over a broad region extending from North Africa to the Middle East (approximately 20°N–40°N, 20°E–60°E). The spatial distribution of the observations is compared to that predicted by the GEOS-Chem model (Figure 1b). Each GEOS-Chem ozone profile has been smoothed by applying the TES averaging kernels and a priori constraint vector [e.g., *Jones et al.*, 2003] for the colocated retrieved TES profile to account for the bias introduced by the averaging kernels and the a priori

$$\hat{\mathbf{x}}_{GCS} = \mathbf{x_a} + \mathbf{A}(\mathbf{x}_{GC} - \mathbf{x_a}), \quad (1)$$

where $\mathbf{A} = \partial\hat{\mathbf{x}}/\partial\mathbf{x}$ is the averaging kernel matrix which describes the sensitivity of the TES ozone estimate to the profile of ozone, $\mathbf{x}_{GC}$ is the nearest GEOS-Chem ozone profile, which has been mapped to the TES pressure grid, and $\hat{\mathbf{x}}_{GCS}$ are the smoothed GEOS-Chem profile. The quantity $\boldsymbol{x_a}$ is the a priori, the constraint vector, which is based on ozone simulations from the MOZART model and is averaged on spatial scales of 10° latitude × 60° longitude. $\hat{\mathbf{x}}_{GCS}$, $\mathbf{x}_{GC}$, and x_a are expressed in terms of the natural logarithm of the volume mixing ratio (VMR). The spatial distribution of the modeled ozone mixing ratio over the Middle East (Figure 1b) is similar to that observed by TES (Figure 1a), with the exception that the modeled ozone enhancement is more pronounced over Saudi Arabia. The ozone distribution is also similar to that obtained by *Li et al.* [2001] using an earlier version of the GEOS-Chem model. The observed ozone peaks at about 120 ppbv, whereas the modeled ozone peaks at about 100 ppbv. Across the extratropics of the northern hemisphere, the model underestimates the ozone abundances compared to the observations, which *Parrington et al.* [2008] attributed to an underestimate of midlatitude NO_x emissions from lightning in this version of the model.

[11] As a result of the limited spatial sampling of the TES observations, Worden et al. (submitted manuscript, 2009) reported that the uncertainty on the mean ozone values over the Middle East is about 10 ppbv in 2006. However, in their

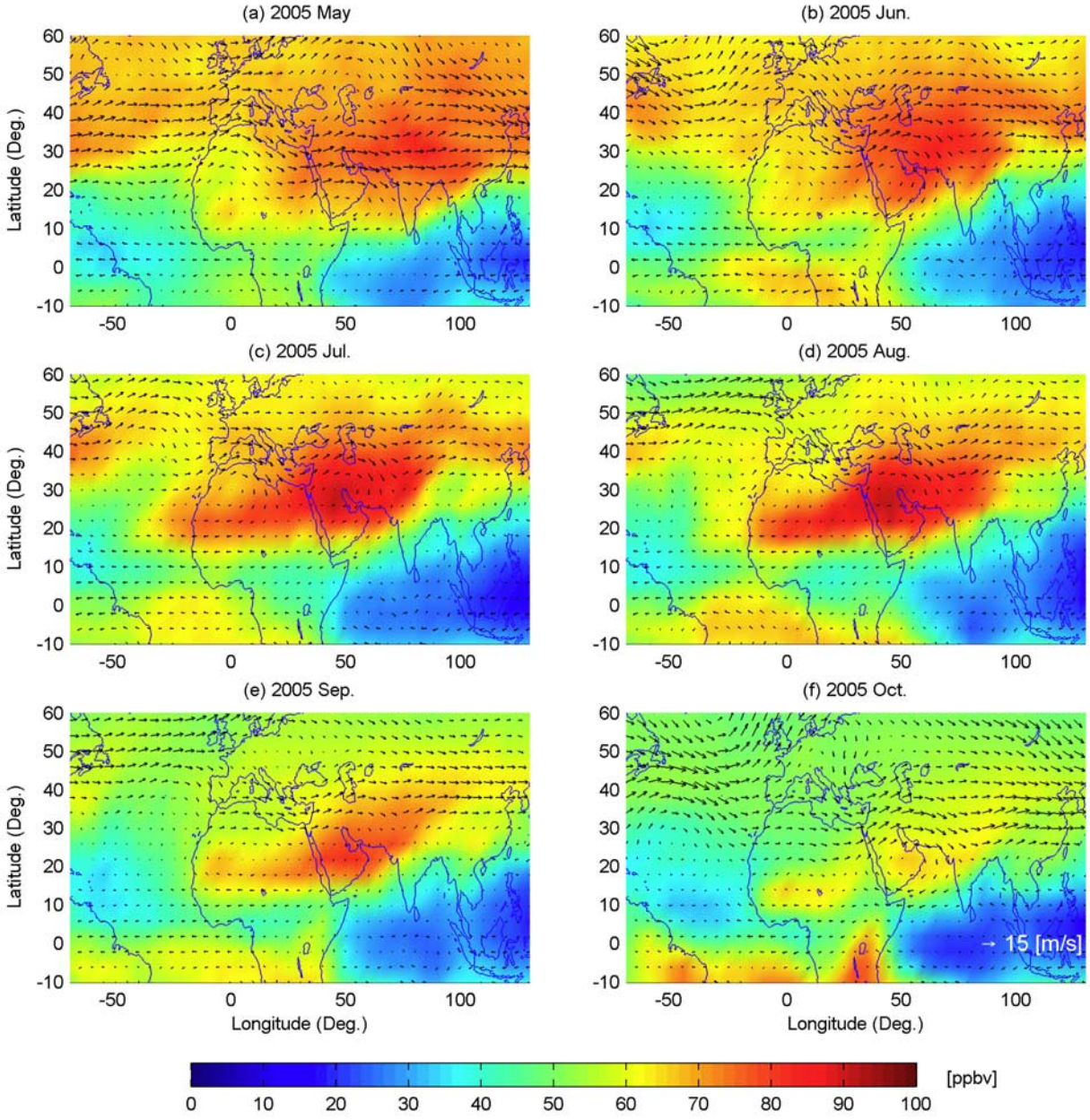

Figure 3. Ozone mixing ratio overlaid with horizontal wind vectors from May to October 2005 at 434 hPa (~6.7 km) in GEOS-Chem.

analysis of TES ozone data, Worden et al. (submitted manuscript, 2009) showed that ozone abundances are enhanced in the middle troposphere over the Middle East and North East Africa for the summers from 2005 through 2007, indicating that the ozone feature is robust.

[12] We examine here the effect of the bias introduced by the varying a priori profiles used in the TES retrievals. Following Worden et al. (submitted manuscript, 2009), we modify the TES ozone retrievals by applying a globally uniform a priori (obtained from a retrieval over the Pacific Ocean). The resulting ozone distribution for July 2005 at 464 hPa is showed in Figure 1c and the overall spatial distribution remains unchanged, although the ozone abundances are slightly lower owing to the lower ozone abundance in the uniform a priori (the O_3 abundance of the uniform a priori averaged over the Middle East (20°N–40°N, 20°E–60°E) is 51.4 ppbv in the compared with 84.3 ppbv of the a priori used in the TES retrievals at 464 hPa shown in Figure 1a). In other words, the a priori bias in the TES retrieval does not significantly affect our conclusion about the spatial distribution of ozone over the Middle East.

3. Summertime Meteorology of the Vicinity of the Middle East

[13] During boreal summer the circulation in the subtropical troposphere of the northern hemisphere is dominated by the influence of the Asian monsoon [*Rodwell and Hoskins*, 1996; *Lelieveld et al.*, 2002; *Lawrence*, 2004]. *Rodwell and Hoskins* [1996] showed that an upper tropospheric anticy-

clone, the so-called Tibetan anticyclone, associated with the Asian Monsoon reflects a Rossby wave response in the atmosphere to the diabatic heating from convection in the monsoon region. The vertical motions associated with this system consist of rising motion in the convection region over South Asia and descending motion in the Rossby wave response region (to the northwest of the convection region). Previous studies have shown that the anticyclone associated with this Rossby wave response has a significant influence on the distribution of trace gases such as O_3, H_2O, and CO in the UTLS [e.g., *Rosenlof et al.*, 1997; *Li et al.* 2005; *Filipiak et al.*, 2005; *Kar et al.*, 2004; *Randel and Park*, 2006; *Park et al.*, 2007]. Observations from the Microwave Limb Sounder (MLS), for example, reveal that within the anticyclone in the UTLS high concentrations of CO are collocated with high H_2O and low O_3, which is attributed to deep convection in the monsoon region [*Park et al.*, 2007].

[14] In the middle troposphere, the descent associated with the monsoon anticyclone is localized over the eastern Mediterranean and over central Asia (near the Caspian and Aral Seas) [*Rodwell and Hoskins*, 1996]. The interaction of the mean flow with the Atlas Mountains of northern Algeria and the Zagros Mountains in Iran induces anticyclonic flow in these regions, and equatorward transport of cold air on the eastern flanks of the anticyclones help localize and intensify the descent over the eastern Mediterranean and central Asia [*Rodwell and Hoskins*, 1996]. The air that is transported equatorward sinks adiabatically along isentropes, which reduces its relative humidity, and thereby contributes to the aridity observed in these regions. Diabatic cooling in the descent regions further enhances the descent, enabling the air masses to descend faster than the isentropic surfaces [*Rodwell and Hoskins*, 1996; *Eshel and Farrell*, 2000].

[15] The vertical velocity and wind vectors in the middle troposphere from the GEOS-4 meteorological fields in the GEOS-Chem model are shown in Figure 2. The model captures the centers of descent over the eastern Mediterranean and over central Asia identified by *Rodwell and Hoskins* [1996]. Across tropical Africa the influence of the Intertropical Convergence Zone (ITCZ) is present in the model as a band of rising air along 10° N. The anticyclones over northwestern Africa (near the Atlas Mountains, referred as the Saharan anticyclone) and over southwestern Iran (near the Zagros Mountains, referred as the Iranian high or Arabian anticyclone) [*Zhou and Li*, 2002; *Lawrence*, 2004] in GEOS-4 are also shown in Figure 2. The northwesterly flow on the eastern flank of the anticyclones coincides with the regions of strongest descent, as predicted by *Rodwell and Hoskins* [1996].

[16] In the lower troposphere, the meteorological conditions across the Mediterranean and Middle East are characterized by a thermal low that extends from the Persian Gulf across Iraq and into Turkey, and which is capped at about 850 hPa (1400–1500 m) [*Bitan and Sa'Aroni*, 1992] by a thermal inversion that is formed by the warming from the subsidence extending down from the middle and upper troposphere. Associated with this "Persian trough" is a northwesterly flow of cool air from Europe in the eastern Mediterranean [*Ziv et al.*, 2004]. Because of the thermal inversion, local anthropogenic emissions from North Africa and the Middle East are not expected to provide a significant contribution to ozone production in the middle and upper troposphere. *Kar et al.* [2006], however, reported that observations of atmospheric CO from the Measurements of Pollution In the Troposphere (MOPITT) reveal a persistent enhancement in CO over the Zagros Mountains, which they argued is linked to mountain venting which transports boundary layer air into the free troposphere, suggesting that surface pollution could contribute to the ozone enhancement observed in the region.

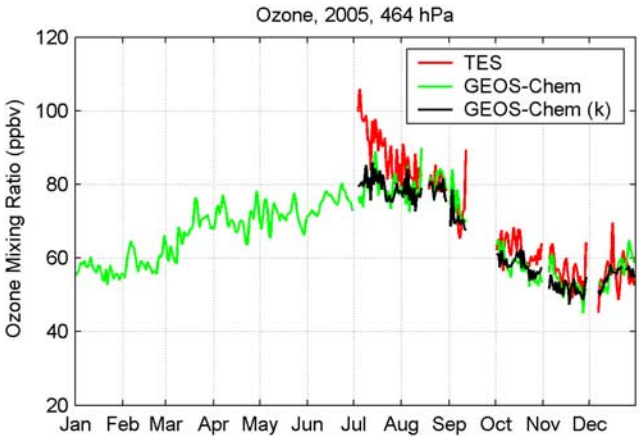

Figure 4. Daily ozone abundance averaged over the Middle East (20°N–40°N, 30°N–60°E) at 464 hPa from TES (in red), the GEOS-Chem model (in green), and the GEOS-Chem model smoothed with the TES averaging kernels and a priori (see equation (1), in black). Continuous TES data are available for the area from 1 July to 31 December 2005.

4. GEOS-Chem Simulations of O_3, CO, and H_2O Over the Middle East and North Africa

[17] The seasonal evolution of the atmospheric circulation and the ozone distribution at 434 hPa over North Africa and the Middle East from GEOS-Chem is shown in Figure 3. In May 2005 (Figure 3a) the flow is primarily westerly, with high ozone across the midlatitudes, reflecting the well-known midlatitude springtime maximum in ozone [*Wang et al.*, 1998a]. By June 2005 the anticyclone over the Persian Gulf forms (Figure 3b) and associated with it are relatively high abundances of ozone across the Middle East and central Asia. By July and August 2005 (Figures 3c and 3d), the anticyclones over the Persian Gulf and northwestern Africa are well established in the model and the region of high ozone extends from the Middle East, across North Africa, and over the eastern subtropical Atlantic. In July, over central Asia, on the eastern flank of the anticyclone over the Persian Gulf, the enhanced ozone extends eastward into central Asia. This eastward extension of the region of enhanced ozone across Mongolia and southern Russia in July 2005 can also be seen in the TES observations in Figure 1a. After September, ozone concentrations across the region decrease dramatically as the anticyclones weakened and the region is ventilated more effectively (Figures 3e and 3f). The seasonal cycle of the ozone enhancement is better illustrated in Figure 4, which shows the time series of observed and modeled ozone over

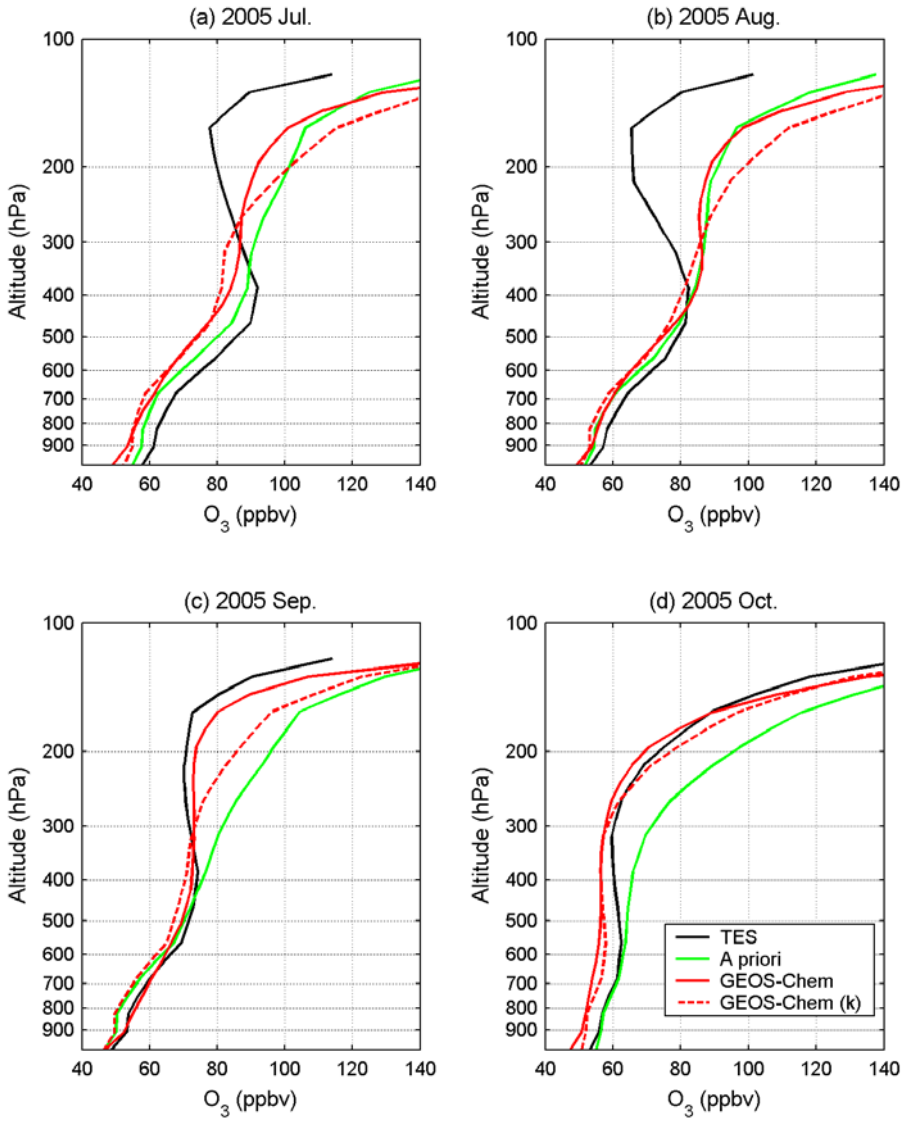

Figure 5. Monthly mean ozone vertical profiles of TES, the a priori, GEOS-Chem, and GEOS-Chem smoothed with the local TES averaging kernels (see equation (1)) in the Middle East region in 2005 (a) July, (b) August, (c) September, and (d) October.

the Middle East (20°N–40°N, 30°E–60°E) at 464 hPa in 2005. For comparison we show the original modeled ozone abundances and the modeled fields sampled along the TES orbit and transformed using the TES averaging kernels and a priori profiles. Both TES and GEOS-Chem show a similar seasonal dependence with a correlation of coefficient of r = 0.94. The modeled and observed ozone abundances decrease from a maximum of about 80–90 ppbv in July and August to a minimum of about 50–60 ppbv in winter. In contrast, ozone abundances in the extratropical troposphere (30°N–60°N) in the midtroposphere are at a maximum in April in the model.

[18] The vertical structure of the modeled and observed ozone, averaged over the Middle East (20°N–40°N, 30°E–60°E) is shown in Figure 5. The ozone enhancement as observed by TES is localized in the middle troposphere around 400 hPa and is at a maximum in July (Figure 5a). The observed ozone enhancement peaks at about 90 ppbv in July 2005 and is much less pronounced by October 2005 (~60 ppbv) (Figure 5d), reflecting the weakening of the anticyclone over the Arabian Peninsula in boreal fall. This seasonality of the ozone profile is similar to that measured over Teheron (35°N, 51°E) and Dubai (25°N, 55°E) by the MOZAIC program [*Li et al.*, 2001; Worden et al., submitted manuscript, 2009]. In the ozonesonde measurements at Isfahan (32.5°N, 51.7°E), ozone abundances near 400 hPa were over 100 ppbv on 14 August 2005, but were significantly lower by September 2005 (not shown). The vertical structure of the enhancement is much less pronounced in the model than in the TES observations. The ozone abundances in the upper troposphere in the model are significantly higher than those retrieved from TES in July and August 2005. In contrast, by October 2005 the modeled vertical distribution of ozone is in better agreement with the TES observations. In summer, the model simulation overestimates ozone in the upper troposphere with both the Linoz and Synoz stratospheric boundary conditions.

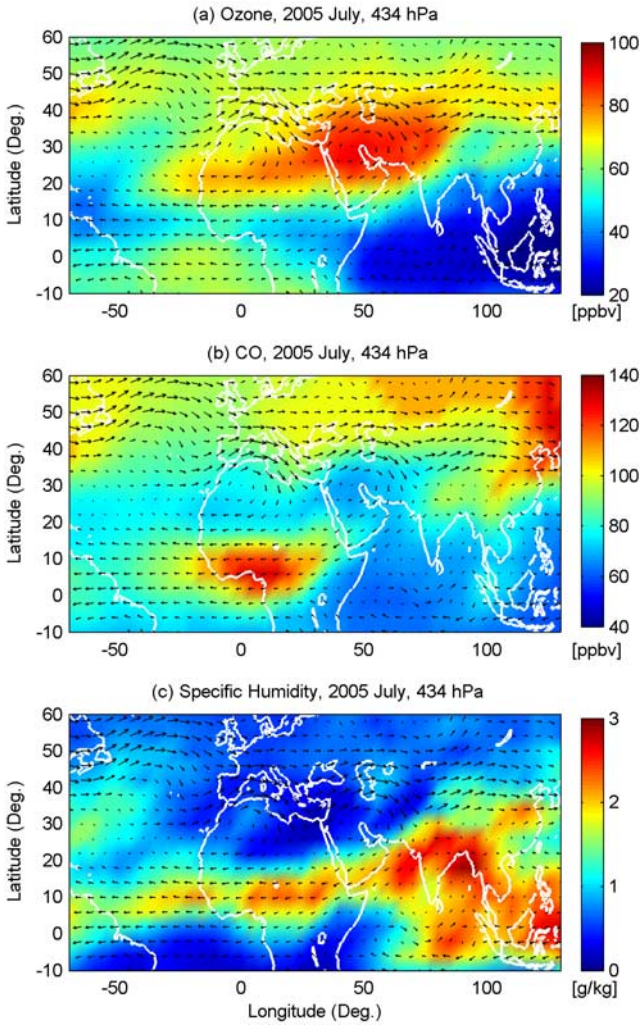

Figure 6. GEOS-Chem simulated: (a) ozone mixing ratio, (b) CO mixing ratio, and (c) specific humidity at 434 hPa (~6.7 km) in July 2005. All are overlaid with the wind field at this altitude. The magnitude of the wind speed is the same as in Figure 2.

[19] In July 2005, the well-developed anticyclones over northwestern Africa and the Persian Gulf, together with the subtropical westerly jet over the Mediterranean in the north and the ITCZ to the south, isolate northeast Africa and the Middle Eastern middle troposphere. In this region, enhanced ozone in the middle troposphere in the model is strongly correlated with low specific humidity and low atmospheric CO (Figure 6). The low specific humidity in the model is consistent with strong descent from the upper troposphere over the region. In the middle troposphere (6–8 km) over northeast Africa (15°N–30°N, 0°E–35°E), the correlation between O_3 and CO is $r = -0.87$ and the correlation between O_3 and H_2O is $r = -0.84$. For the Middle East (15°N–30°N, 30°E–60°E), the correlation is $r = -0.69$ between O_3 and CO and $r = -0.70$ between O_3 and H_2O. The O_3/CO correlations suggest three distinct regions across North Africa and the Middle East: high ozone and high CO north of the westerly jet, high ozone and low CO south of the jet, and low ozone and high CO in the vicinity of the ITCZ over central Africa. North of the westerly jet the positive correlation between ozone and CO reflects the influence of anthropogenic emissions on the distribution of ozone and CO, whereas over tropical Africa, the high CO and low ozone is due the influence of rapid convective transport of surface emissions of CO. Similarly, over central Africa and southern Asia, high abundances of H_2O coincide with low ozone owing to the influence of convective transport within the ITCZ.

[20] The high ozone, low CO, and low specific humidity that characterizes the Middle East in the middle troposphere is in contrast to the conditions in the UTLS region, where, as discussed above, the large-scale extension of the Asian monsoon anticyclone is associated with high CO, high specific humidity and low ozone. In the upper troposphere the model simulates a broad maximum in CO extending from East Africa to East Asia (not shown), in agreement with previous studies of the Asian monsoon anticyclone [e.g., *Lawrence et al.*, 2003; *Li et al.*, 2005; *Kar et al.*, 2004; *Randel and Park*, 2006]. However, the model does not simulate a well-defined ozone within the anticyclone region as previously observed [e.g., *Park et al.*, 2007]. This bias may be related to the overestimate of ozone in the model, relative to TES observations, in the UTLS over the Middle East, as shown in Figure 5a and in work by Worden et al. (submitted manuscript, 2009), or due to discrepancies in the strength of deep convection over South Asia in the model.

5. Sources of Ozone Over the Middle East and North Africa

5.1. Ozone Photochemical Production

[21] Photochemistry provides a net source of ozone in the upper troposphere in summer [e.g., *Wang et al.*, 1998b; *von Kuhlmann et al.*, 2003], whereas it is generally a net sink for ozone in the lower troposphere, in the absence of anthropogenic emissions, because of the high loss rates of ozone in the boundary layer. The net photochemical production rate of ozone as a function of longitude and altitude in the subtropics (20°N–30°N) is shown in Figure 7. In the subtropical middle and upper troposphere in July, the net photochemical production of ozone is at a maximum over South Asia (60°E–90°E), East Asia (90°E–120°E), and over southern North America (60°W–120°W). *Li et al.* [2001] found that emissions of NO_x from lightning provides an important source of ozone over the Middle East. The maxima in the ozone production rates shown in Figure 7 are colocated with regions of strong emissions of NO_x from lightning (not shown), with South Asia providing the dominant source of lightning NO_x in the subtropics between 20 and 30°N in the model. As the Middle East is strongly influenced by transport of pollution from Asia [*Li et al.* 2001], accurately reproducing the horizontal and vertical distribution of O_3 over the Middle East will depend on correctly capturing the magnitude and spatial distribution of the lightning NO_x source over South Asia. *Sauvage et al.* [2007] modified the lightning NO_x source in a version of the GEOS-Chem model, using data from the Optical Transient Detector (OTD) and Lightning Imaging Sensor (LIS) and found that lightning NO_x emissions were lower in summer over the Asian monsoon region in the model, with a consequent reduction in the overestimate of ozone in the middle and upper troposphere in the model relative to ozonesonde measurements over Dubai, in the Middle East.

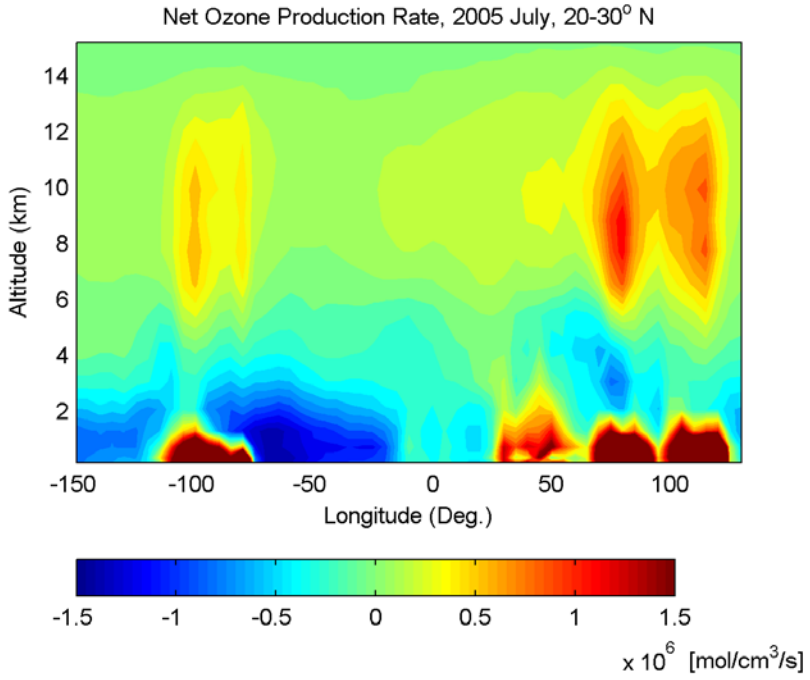

Figure 7. GEOS-Chem simulated net ozone production rate for 2005 July averaged over 20°N–30°N. The altitude for the elevated ozone in Figure 1 is around 6–8 km.

[22] As shown in Figure 7, across North Africa (0°–30°E) the net rate of production of ozone is relatively uniform. At 8 km the mean net production rate for ozone between is about 2×10^5 molec. cm^{-3} s^{-1}, which is about 2 ppbv d^{-1}. The ozone enhancement is confined to the middle and upper troposphere because of the strong photochemical sink of ozone in the lower troposphere. The lifetime of ozone over northeast Africa decreases from about 50 days at 9 km to less than 10 days at 4 km. Confinement of the region due to the presence of the Arabian anticyclone and weak winds over northeastern Africa are therefore critical for enabling the buildup of ozone. Ozone that is produced in the middle and upper troposphere over North Africa and the Middle East is rapidly destroyed in the lower troposphere as a result of the descent in the region. Accurately reproducing the ozone distribution across North Africa and the Middle East will depend on correctly capturing the descent in the region and the relative strengths of the anticyclones over the Persian Gulf and northwestern Africa.

5.2. Tagged Ozone Simulation

[23] We conduct a tagged ozone simulation using the GEOS-Chem model to quantify the contribution of in situ production and long-range transport of ozone to the ozone enhancement over the Middle East and North Africa. The tagged ozone simulation was conducted using archived 24-h-averaged odd oxygen ($O_x \equiv O + O_3 + NO_2 + 2NO_3$) production rates and loss frequencies from a full chemistry run of the model. In our analysis, we focus on the two receptor regions where the ozone abundance is high: the Middle East (15°N–35°N, 30°E–60°E) and North Africa (15°N–35°N, 0°–30°E). The source regions include Asia (0°–35°N, 60°E–145°E), North America (15°N–70°N, 125°W–65°W), equatorial Africa (20°S–15°N, 25°W–55°E), and Europe (40°N–70°N, 15°W–40°E). Each region is divided into three layers in altitude: an upper tropospheric layer (300 hPa to tropopause), a middle tropospheric layer (300–700 hPa), and the boundary layer (pressures greater than 700 hPa). Two additional source regions are the rest of the world in the troposphere and the stratosphere.

[24] Figure 8 shows the seasonal variation of the fractional contribution of ozone from the different source regions to the ozone abundances at about 434 hPa over the Middle East and North Africa. Over the Middle East (Figure 8a), both in situ production and transport of ozone from Asia are the major sources of ozone in the middle troposphere in July and August (contributing about 30–35% each). In contrast, the influences of the other regions are at a minimum (5–10% each) (Figure 8b), reflecting the isolation of the region due to the presence of the summertime Arabian anticyclone. Over North Africa (Figure 8c) the contribution from in situ production and transport from Asia in summer is reduced to ~20% and ~15%, respectively, while the contribution from transport from other source regions becomes larger, especially from North America (~10%) and the rest of the world (~20%). Table 1 provides a summary of the fractional contribution of the different source regions to the ozone budget in July, partitioning the contribution from each region into components from the upper troposphere, the middle troposphere and the boundary layer. Over the Middle East, for example, the contribution of ozone transported from the upper troposphere, the middle troposphere, and the boundary layer of Asia are estimated to be 13%, 10%, and 8%, respectively. For the in situ source of ozone in the Middle East, the dominant contribution is from ozone produced in the middle troposphere (16%), although ozone produced in the upper troposphere and in the boundary each contributed about 8%. A recent study by

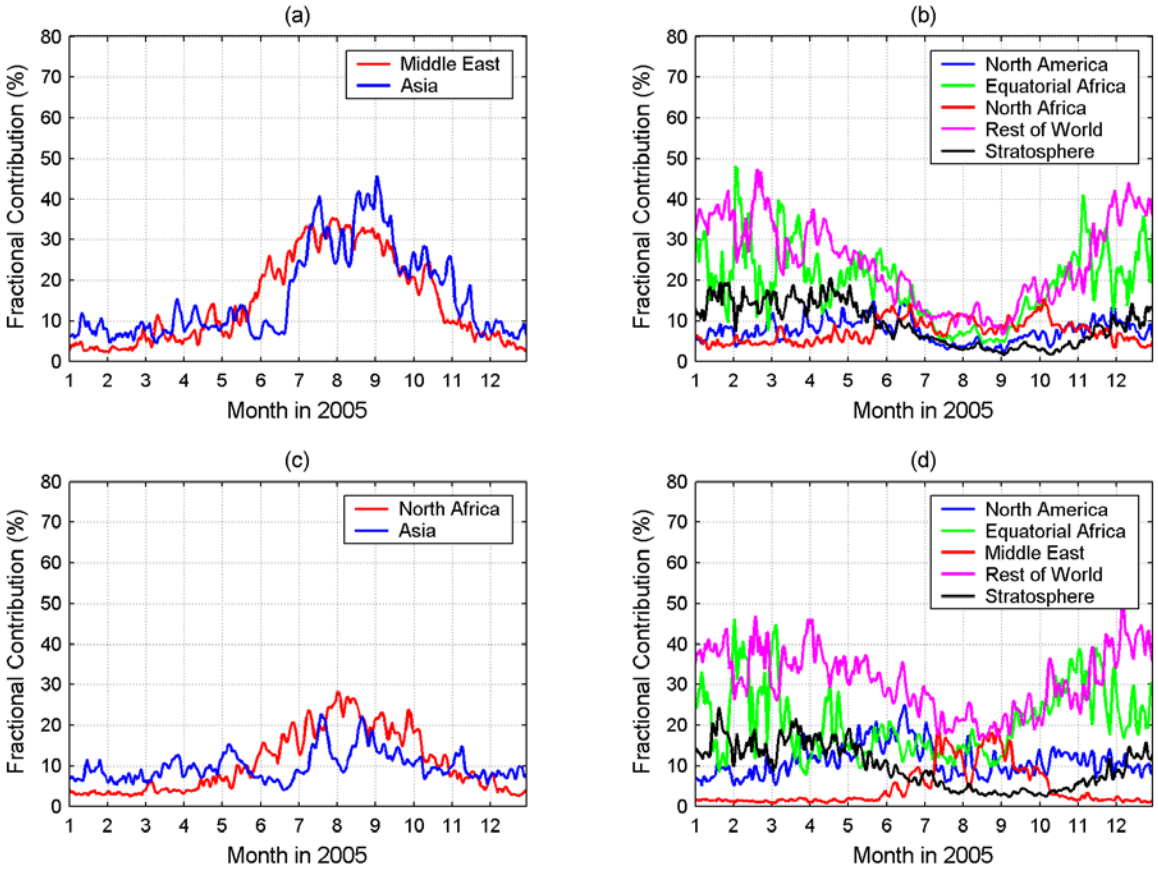

Figure 8. The fractional contribution from different source regions to the ozone abundance in (a, b) the Middle East and (c, d) North Africa at 434 hPa in 2005. (left) Contribution from local in situ production (in red) and from ozone transported from Asia (in blue). (right) Fractional contribution from the other source regions (see region domains in section 5.2). The European influence is small and thus is excluded here.

Lelieveld et al. [2008] revealed high surface ozone concentrations in the Middle East during summer, partly due to anthropogenic surface emission. Overall, ozone from the boundary layer contributes ~23% and 21% to midtropospheric ozone in the Middle East and North Africa, respectively.

[25] Figure 9 shows examples of the distinct spatial patterns the ozone abundances at 434 hPa in July 2005, which are attributed to the ozone produced in the middle troposphere of the Middle East (Figure 9a), the upper troposphere of Asia (Figure 9b), the North American boundary layer (Figure 9c), and the stratosphere (Figure 9d). As noted above, in situ production in the middle troposphere of the Middle East and ozone transported from the Asian upper troposphere are the two dominant contributions to ozone abundances in the Middle East. The ozone produced in the midtroposphere in the Middle East is confined over Saudi Arabia (Figure 9a), largely owing to the presence of the Arabian anticyclone over the Persian Gulf around this altitude (see Figure 3c), although net ozone production rate in the region is even somewhat lower than in the surrounding areas at this altitude (not shown). The ozone from the Asian upper troposphere is transported westward between 20°N and 35°N and descends to the midtroposphere most strongly over the Middle East and central Asia (Figure 9b). This is consistent with the discussion of the meteorological and chemical contexts in sections 3

Table 1. Fractional Contribution to the Ozone Abundance in the Middle East and North Africa at 434 hPa in 2005 July From a GEOS-Chem Tagged Ozone Simulation[a]

Receptor Region	Source Region	UT[b]	MT[b]	BL[b]	Total
Middle East	Asia	13	10	8	31
	North America	1	1	2	4
	Europe	<1	<1	<1	<1
	Equatorial Africa	3	2	3	8
	North Africa	5	3	1	9
	Middle East[c]	8	16	8	32
	Rest of world				11
	Stratosphere				5
North Africa	Asia	6	4	4	14
	North America	3	3	5	11
	Europe	1	1	1	2
	Equatorial Africa	4	6	4	13
	North Africa[c]	3	5	4	12
	Middle East	5	12	3	20
	Rest of world				22
	Stratosphere				6

[a]Fractional contribution given as percent.
[b]UT denotes the upper troposphere (300 hPa to the tropopause), MT is the middle troposphere (700–300 hPa), and BL is the boundary layer (>700 hPa).
[c]This is the local ozone production.

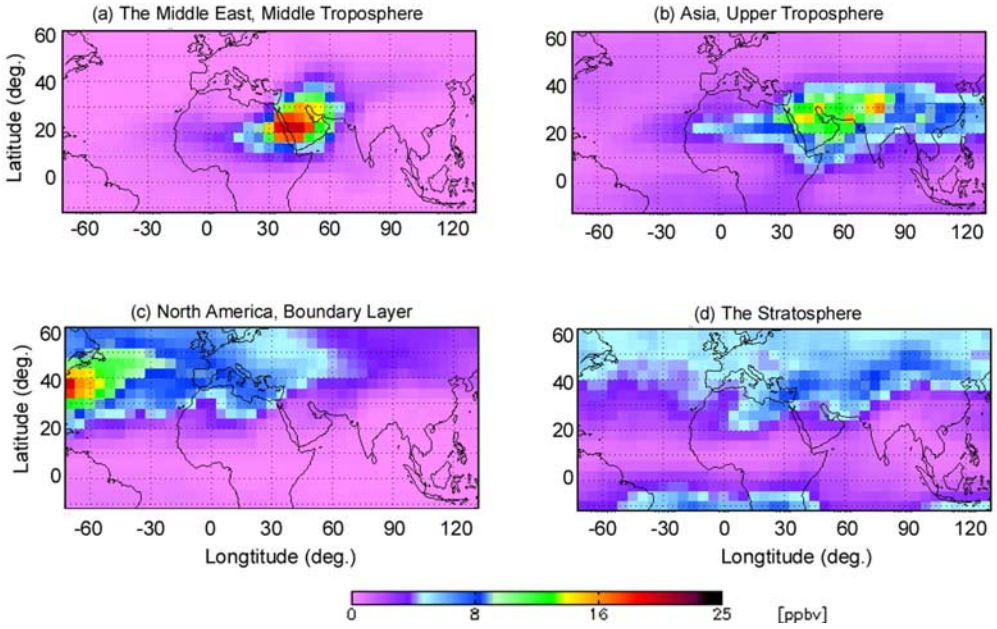

Figure 9. Ozone mixing ratio in July 2005 at 434 hPa that is attributed to the ozone production in (a) the Middle Eastern middle troposphere, (b) the Asian upper troposphere, (c) the North American boundary layer, and (d) the stratosphere.

and 5.1. The contributions of ozone from the North American boundary layer and from the stratosphere (Figures 9c and 9d) are relatively small, less than 5% to the total ozone abundance over the Middle East. The stratospheric ozone contribution is largest in the regions of strong descent, such as over northeastern Africa and central Asia, whereas the North American source is transported from the west and is dominant over the eastern Mediterranean.

[26] The different pathways for transport of ozone over North Africa and the Middle East are shown in the plots of the zonal flux of ozone in Figure 10. In the northern region of the domain (Figure 10a), transport is primarily westerly, in the vicinity of the westerly jet, whereas in the south (Figure 10c) transport is easterly, capturing the outflow from the Asian monsoon region. Furthermore, Figure 10 reveals that downward transport of ozone is localized in the eastern Mediterranean region in the model and that there is significant upward transport of ozone from the boundary layer into the middle troposphere in the Middle East. This upward transport is strongly influenced by the orography of the region. Over the Zagros Mountains (between 50°E and 60°E in Figures 10a and 10b), there is significant upward transport of ozone extending into the middle troposphere in the model. There is also strong upward transport of ozone over western Saudi Arabia and Yemen, between 40 and 50°E in Figure 10c. This region of upward transport extends along the Asir and Hijaz mountain ranges, along the Red Sea coast of western Saudi Arabia. In fact, the greatest upward flux of ozone in the lower troposphere in the Middle East in the model is located in this region. As shown in Table 1, our tagged ozone analysis indicates that transport of ozone from the boundary layer in the Middle East domain accounts for a large fraction (about 25%) of the total in situ Middle Eastern ozone production to the ozone abundance in the middle troposphere.

[27] Recently, *Tangborn et al.* [2009] showed that the simulation of CO in the GEOS-4 general circulation model at GMAO, with surface emissions and the atmospheric chemistry of CO specified from the GEOS-Chem model, significantly underestimates CO abundances over the Arabia Peninsula compared to observations from SCIAMACHY (Scanning Imaging Absorption Spectrometer for Atmospheric CHartographY) and MOZAIC. Since CO serves as a proxy for the hydrocarbon and combustion-related precursor emissions of ozone, this bias could indicate a significant underestimate of the impact of surface emissions in the Middle East on ozone abundances in the middle troposphere as a result of the strong upward transport shown in Figure 10.

6. Constraints From TES H_2O and HDO/H_2O on the Transport Mechanisms Over the Middle East and North Africa

[28] We examine in this section TES observations of H_2O and HDO to assess the consistency of the model simulation with the constraints from the TES data on the transport pathways over North Africa and the Middle East. Observations of HDO/H_2O are particularly valuable in this context as the isotopic composition of water vapor can be used as an indicator of the source of the vapor, and therefore provides information on the transport pathways of air masses [*Worden et al.*, 2007]. Water vapor becomes more depleted in HDO/H_2O as it undergoes condensation, and as such, the most depleted vapor is that at high latitudes and altitudes in the troposphere or of stratospheric origin. In the case of the latter, water in the lower stratosphere is dominated by a tropospheric source which has undergone an extensive history of condensation as it crosses the tropopause. On the other hand, vapor that has not undergone a history of condensation will appear as relatively enriched in HDO relative to H_2O and indicate an air mass source (either from evaporation from

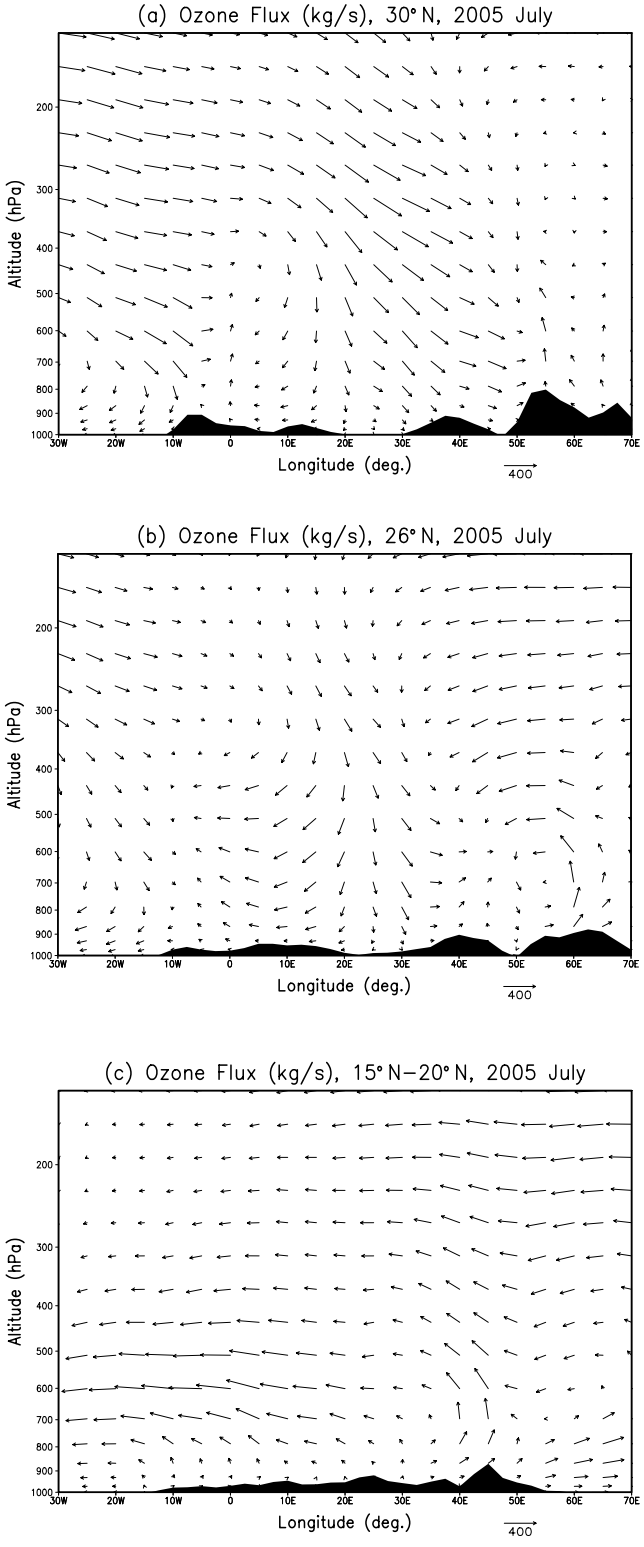

Figure 10. GEOS-Chem simulated ozone flux along (a) 30°N, (b) 26°N, and (c) 15°N–20°N in July 2005.

the ocean or from continental evapotranspiration) near the surface.

[29] Monthly mean TES observations of H_2O for July 2005 are shown in Figure 11a. Low abundances of H_2O are observed across North Africa and the Middle East as expected given the aridity of these regions. The dipole structure in the distribution of H_2O, with high H_2O over South Asia and low H_2O across North Africa and the Middle East, reflects the influence of convective transport over South Asia and subsidence over North Africa and the Middle East [e.g., *Stone et al.*, 2000]. Note that, there are gaps in the H_2O and HDO/H_2O maps shown in Figure 11 due to the low density of reliable H_2O and HDO retrievals. The number of observation per grid box for July 2006 ranges from 2 to 8 over the Middle East and North Africa.

[30] Monthly mean TES observations of HDO/H_2O, presented as δD, are shown in Figure 11b, and reveal a spatial distribution different from that of H_2O. Values of δD are high across much of the region, except over northeastern Africa. The high δD values over northwestern Africa (near Morocco) and the Middle East, in contrast to the lower δD over northeastern Africa (near Egypt), indicates that the origin of the air in these regions is different from that over northeastern Africa. Over the Arabian Peninsula and central Asia, where δD is high, one would expect a strong evapotranspiration source at the surface. As shown in Figure 10, there is significant upward transport of ozone in these regions, associated with the Zagros Mountains in southern Iran and the Asir and Hijaz mountain ranges on the Arabian Peninsula. This upward transport would also provide a source of surface air with high δD to the middle troposphere. Similarly, the high δD values over

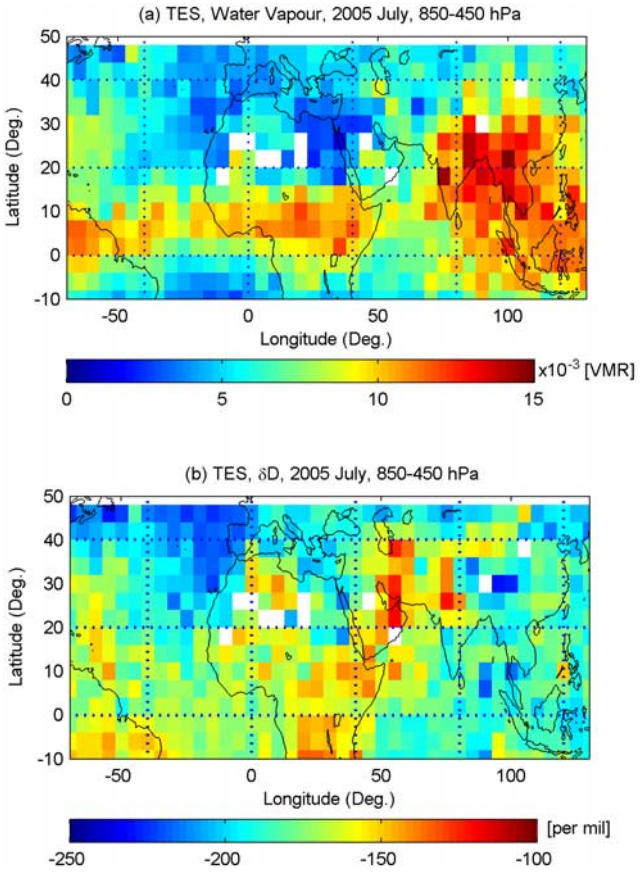

Figure 11. TES observation of (a) H_2O and (b) and δD (HDO/H_2O) for July 2005, averaged over 850–450 hPa. White areas are missing data.

northwestern Africa are consistent with convection and orographic lifting over the Atlas Mountains, which has been reported by *Knippertz et al.* [2003]. This region of convection and orographic lifting in the GEOS-Chem fields is shown in Figure 2 as a region of upward motion extending from Morocco to southern Spain (near 0°E, 35°N), and coincides with region of high δD inferred from the TES data (Figure 11b). This region of upward motion in GEOS-Chem also coincides with low abundances of ozone simulated over northwestern Africa, as shown in Figure 6a.

[31] The region of low δD values over northeastern Africa is coincident with the strong descent over North Africa and the downward transport of ozone shown in Figures 10a and 10b suggests that subsidence from the upper troposphere is responsible for the depleted HDO/H_2O. Since the downward transport is equatorward along the isentropes, the air over eastern North Africa will originate mainly in the extratropical upper troposphere. Indeed, back trajectory analyses conducted using the GEOS-4 meteorological fields (not shown) indicate that air masses over eastern North Africa originate over North America and the western Atlantic and are transported across the northern Atlantic Ocean and up to the high-latitude upper troposphere, followed by equatorward descent over Europe down to the Mediterranean region, accounting for the low δD observed over North Africa by TES. Furthermore, as shown above in our tagged ozone analysis, it is over this region that the contribution of ozone from North America is at a maximum over North Africa and the Middle East.

7. Summary and Conclusions

[32] We used the GEOS-Chem chemical transport model to interpret observations of tropospheric ozone from the Tropospheric Emissions Spectrometer (TES) satellite instrument. Observations from TES reveal elevated ozone in the middle troposphere ($\sim$500–400 hPa) over the vicinity of the Middle East in summer 2005. This enhancement has some similarities to and differences from the "Middle East ozone maximum," previously suggested in a model study by *Li et al.* [2001]. We have examined the mechanism responsible for this "ozone maximum" in the context of the recent TES measurements. In particular, we focused on understanding the influence of long-range transport of ozone and local in situ chemical production on the spatial and temporal variations of tropospheric ozone over the Middle East and North Africa.

[33] We showed that ozone abundances in the middle troposphere across the region are at a maximum in June–August and a minimum in December–February. In summer, the spatiotemporal distribution of ozone across North Africa and the Middle East reflects the influence of the Arabian and Saharan anticyclones, centered in the vicinity of the Zagros and Atlas Mountains, respectively. In the model, the eastern flanks of these anticyclones coincide with regions of descent over North Africa and central Asia (east of the Caspian Sea), as described by *Rodwell and Hoskins* [1996]. In the observations and in the model, we found high concentrations of ozone extending from the Arabian anticyclone region to the coast of northwestern Africa, near the southeastern flank of the Saharan anticyclone, bounded by the ITCZ to the south and the subtropical westerly jet to the north. We showed that in the model, over the Middle East, high ozone abundances in the middle troposphere are correlated with low specific humidity and low atmospheric CO. This is in contrast to conditions in the outflow region of the Asian monsoon in the UTLS where low ozone is correlated with high specific humidity and high CO.

[34] We conducted a tagged ozone simulation using the GEOS-Chem model to quantify the contribution of in situ production of ozone and transport of ozone to the ozone enhancement. We found that in situ production and transport from Asia provided comparable contributions of 30–35% to the ozone over the Middle East in July 2005. Over North Africa, the contribution to the total ozone in the middle troposphere from in situ production was dominant (at about 20%), with transport from Asia, North America, and equatorial Africa each contributing about 10–15% of the total. Over both North Africa and the Middle East, the contribution of European emissions to the ozone enhancement was less than 2%, reflecting the confinement of European pollution to the lower troposphere. We found that the North American influence was at a maximum over North Africa, in the region of strong descent.

[35] Although the lower troposphere in the Middle East in summer is capped by a thermal inversion, we found that ozone produced in the boundary layer of the Middle East accounted for about 25% of the local Middle Eastern contribution to the ozone enhancement in the middle troposphere. We showed that this transport of boundary layer air to the middle troposphere is consistent with the distribution of HDO retrieved from the observations from TES. Examination of TES H_2O and HDO/H_2O showed that although H_2O is low across North Africa and the Middle East, high δD values over the Middle East and central Asia indicate significant isotopic enrichment of H_2O in these regions which we argued is due to the transport of boundary layer air into the middle troposphere by orographic lifting over the Zagros Mountains in Iran and along the Asir and Hijaz mountain ranges in Saudi Arabia.

[36] Our analysis showed that the model overestimates ozone in the middle and upper troposphere over the Middle East. This bias may be due to an overestimate of in situ production of ozone in the middle and upper troposphere over the Middle East or to discrepancies in the description of the outflow of ozone precursors from the Asian monsoon region in the model. Accurately simulating the magnitude and spatial distribution of the ozone enhancement will require properly reproducing ozone production rates in the middle and upper troposphere and characterizing the atmospheric circulation response in the Middle East to the Asian Monsoon. Our results also suggested that although the focus on the ozone enhancement in the Middle East has been primarily in the context of long-range transport, further work is needed to better quantify the influence of surface emissions on the ozone budget over North Africa and the Middle East. High-resolution regional chemical transport models would be especially useful, as they should more accurately capture the impact of orography on the atmospheric circulation over this region.

[37] **Acknowledgments.** This work was supported by funding from the Natural Sciences and Engineering Research Council of Canada (NSERC) and the Canadian Foundation for Climate and Atmospheric Sciences. Liu thanks additional funds from Canadian Space Agency and Environment Canada. Worden's work was performed at the Jet Propulsion Laboratory, California Institute of Technology under contracts from the

National Aeronautics and Space Administration. We are grateful to Mark Lawrence and two anonymous reviewers for their valuable comments. The GEOS-Chem model is managed at Harvard University with support from the NASA Atmospheric Chemistry Modeling and Analysis Program. TES data were obtained from the NASA Langley Research Center Atmospheric Science Data Center.

References

Beer, R., T. A. Glavich, and D. M. Rider (2001), Tropospheric emission spectrometer for the earth observing system's Aura satellite, *Appl. Opt.*, *40*, 2356–2367, doi:10.1364/AO.40.002356.

Benkovitz, C. M., M. T. Scholtz, J. Pacyna, L. Tarrasón, J. Dignon, E. C. Voldner, P. A. Spiro, J. A. Logan, and T. E. Graedel (1996), Global gridded inventories of anthropogenic emissions of sulfur and nitrogen, *J. Geophys. Res.*, *101*(D22), 29,239–29,253, doi:10.1029/96JD00126.

Berntsen, T., S. Karlsdóttir, and D. Jaffe (1999), Influence of Asian emissions on the composition of air reaching the North Western United States, *Geophys. Res. Lett.*, *26*(14), 2171–2174, doi:10.1029/1999GL900477.

Bey, I., D. J. Jacob, R. M. Yantosca, J. A. Logan, B. D. Field, A. M. Fiore, Q. Li, H. Y. Liu, L. J. Mickley, and M. G. Schultz (2001), Global modeling of tropospheric chemistry with assimilated meteorology: Model description and evaluation, *J. Geophys. Res.*, *106*(D19), 23,073–23,095, doi:10.1029/2001JD000807.

Bitan, A., and H. Sa'Aroni (1992), The horizontal and vertical extension of the Persian Gulf pressured trough, *Int. J. Climatol.*, *12*, 733–747, doi:10.1002/joc.3370120706.

Bowman, K. W., et al. (2006), Tropospheric emission spectrometer, retrieval method and error analysis, *IEEE Trans. Geosci. Remote Sens.*, *44*, 1297–1307, doi:10.1109/TGRS.2006.871234.

Duncan, B. N., and I. Bey (2004), A modeling study of the export pathways of pollution from Europe: Seasonal and interannual variations (1987–1997), *J. Geophys. Res.*, *109*, D08301, doi:10.1029/2003JD004079.

Duncan, B. N., R. V. Martin, A. C. Staudt, R. Yevich, and J. A. Logan (2003), Interannual and seasonal variability of biomass burning emissions constrained by satellite observations, *J. Geophys. Res.*, *108*(D2), 4100, doi:10.1029/2002JD002378.

Duncan, B. N., J. J. West, Y. Yoshida, A. M. Fiore, and J. R. Ziemke (2008), The influence of European pollution on ozone in the Near East and northern Africa, *Atmos. Chem. Phys.*, *8*, 2267–2283.

Eshel, G., and B. F. Farrell (2000), Mechanisms of eastern Mediterranean rainfall variability, *J. Atmos. Sci.*, *57*, 3219–3232, doi:10.1175/1520-0469(2000)057<3219:MOEMRV>2.0.CO;2.

Filipiak, M. J., R. S. Harwood, J. H. Jiang, Q. Li, N. J. Livesey, G. L. Manney, W. G. Read, M. J. Schwartz, J. W. Waters, and D. L. Wu (2005), Carbon monoxide measured by the EOS Microwave Limb Sounder on Aura: First results, *Geophys. Res. Lett.*, *32*, L14825, doi:10.1029/2005GL022765.

Fiore, A. M., D. J. Jacob, I. Bey, R. M. Yantosca, B. D. Field, A. C. Fusco, and J. G. Wilkinson (2002), Background ozone over the United States in summer: Origin, trend, and contribution to pollution episodes, *J. Geophys. Res.*, *107*(D15), 4275, doi:10.1029/2001JD000982.

Fishman, J. A. W. Wozniak, and J. K. Creilson (2003), Global distribution of tropospheric ozone from satellite measurements using the empirically corrected tropospheric ozone residual technique: Identification of the regional aspects of air pollution, *Atmos. Chem. Phys.*, *3*, 890–907.

Hudman, R. C., et al. (2007), Surface and lightning sources of nitrogen oxides over the United States: Magnitudes, chemical evolution and outflow, *J. Geophys. Res.*, *112*, D12S05, doi:10.1029/2006JD007912.

Jaeglé, L., D. A. Jaffer, H. U. Price, P. Weiss-Penzias, P. I. Palmer, M. J. Evans, D. J. Jacob, and I. Bey (2003), Sources and budgets for CO and O_3 in the northeastern Pacific during the spring of 2001: Results from the PHOBEA-II Experiment, *J. Geophys. Res.*, *108*(D20), 8802, doi:10.1029/2002JD003121.

Jones, D. B. A., K. W. Bowman, P. I. Palmer, J. R. Worden, D. J. Jacob, R. N. Hoffman, I. Bey, and R. M. Yantosca (2003), Potential of observations from the Tropospheric Emission Spectrometer to constrain continental sources of carbon monoxide, *J. Geophys. Res.*, *108*(D24), 4789, doi:10.1029/2003JD003702.

Kar, J., C. R. Trepte, L. W. Thomason, J. M. Zawodny, D. W. Cunnold, and H. J. Wang (2002), On the tropospheric measurements of ozone by the Stratospheric Aerosol and Gas Experiment II (SAGE II, version 6.1) in the tropics, *Geophys. Res. Lett.*, *29*(24), 2208, doi:10.1029/2002GL016241.

Kar, J., et al. (2004), Evidence of vertical transport of carbon monoxide from measurements of pollution in the troposphere (MOPITT), *Geophys. Res. Lett.*, *31*, L23105, doi:10.1029/2004GL021128.

Kar, J., J. R. Drummond, D. B. A. Jones, J. Liu, F. Nichitiu, J. Zou, J. C. Gille, D. P. Edwards, and M. N. Deeter (2006), Carbon monoxide (CO) maximum over the Zagros mountains in the middle east: Signature of mountain venting?, *Geophys. Res. Lett.*, *33*, L15819, doi:10.1029/2006GL026231.

Knippertz, P., A. H. Fink, A. Reiner, and P. Speth (2003), Three later summer/early autumn cases of tropical-extratropical interactions causing precipitation in northwest Africa, *Mon. Weather Rev.*, *131*, 116–135, doi:10.1175/1520-0493(2003)131<0116:TLSEAC>2.0.CO;2.

Lawrence, M. G. (2004), Export of air pollution from southern Asia and its large-scale effects, in *Inter-continental Transport of Air Pollution*, edited by A. Stohl, pp. 131–172, Springer, New York.

Lawrence, M. G., et al. (2003), Global chemical weather forecasts for field campaign planning: Predictions and observations of large-scale features during MINOS, CONTRACE, and INDOEX, *Atmos. Chem. Phys.*, *3*, 267–289.

Lelieveld, J., et al. (2002), Global air pollution crossroads over the Mediterranean, *Science*, *298*, 794–799, doi:10.1126/science.1075457.

Lelieveld, J., P. Hoor, P. Jöckel, A. Pozzer, P. Hadjinicolaou, and J.-P. Cammas (2008), Severe ozone air pollution in the Persian Gulf region, *Atmos. Chem. Phys. Discuss.*, *8*, 17,739–17,762.

Li, Q., et al. (2001), A tropospheric ozone maximum over the Middle East, *Geophys. Res. Lett.*, *28*(17), 3235–3238, doi:10.1029/2001GL013134.

Li, Q. B., et al. (2002), Transatlantic transport of pollution and its effects on surface ozone in Europe and North America, *J. Geophys. Res.*, *107*(D13), 4166, doi:10.1029/2001JD001422.

Li, Q., et al. (2005), Convective outflow of South Asian pollution: A global CTM simulation compared with EOS MLS observations, *Geophys. Res. Lett.*, *32*, L14826, doi:10.1029/2005GL022762.

Liu, X. K., et al. (2006), First directly retrieved global distribution of tropospheric column ozone from GOME: Comparison with the GEOS-CHEM model, *J. Geophys. Res.*, *111*, D02308, doi:10.1029/2005JD006564.

Martin, R. V., et al. (2002), Interpretation of TOMS observations of tropical tropospheric ozone with a global model and in situ observations, *J. Geophys. Res.*, *107*(D18), 4351, doi:10.1029/2001JD001480.

McLinden, C. A., S. O. Olsen, B. Hannegan, O. Wild, and M. J. Prather (2000), Stratospheric ozone in 3-D models: A simple chemistry and the cross-tropopause flux, *J. Geophys. Res.*, *105*(D11), 14,654–14,665.

Nassar, R., et al. (2008), Validation of Tropospheric Emission Spectrometer (TES) nadir ozone profiles using ozonesonde measurements, *J. Geophys. Res.*, *113*, D15S17, doi:10.1029/2007JD008819.

Park, M., W. J. Randel, D. E. Kinnison, R. R. Garcia, and W. Choi (2004), Seasonal variation of methane, water vapor, and nitrogen oxides near the tropopause: Satellite observations and model simulations, *J. Geophys. Res.*, *109*, D03302, doi:10.1029/2003JD003706.

Park, M., W. J. Randel, A. Gettelman, S. T. Massie, and J. H. Jiang (2007), Transport above the Asian summer monsoon anticyclone inferred Aura Microwave Limb Sounder tracers, *J. Geophys. Res.*, *112*, D16309, doi:10.1029/2006JD008294.

Parrington, M., D. B. A. Jones, K. W. Bowman, L. W. Horowitz, A. M. Thompson, D. W. Tarasick, and J. C. Witte (2008), Estimating the summertime tropospheric ozone distribution over North America through assimilation of observations from the Tropospheric Emission Spectrometer, *J. Geophys. Res.*, *113*, D18307, doi:10.1029/2007JD009341.

Pickering, K. E., Y. Wang, W. Tao, C. Price, and J.-F. Müller (1998), Vertical distributions of lightning NO_x for use in regional and global chemical transport models, *J. Geophys. Res.*, *103*(D23), 31,203–31,216, doi:10.1029/98JD02651.

Price, C., and D. Rind (1992), A simple lightning parameterization for calculating global lightning distributions, *J. Geophys. Res.*, *97*(D9), 9919–9933.

Randel, W. J., and M. Park (2006), Deep convective influence on the Asian summer monsoon anticyclone and associated tracer variability observed with Atmospheric Infrared Sounder (AIRS), *J. Geophys. Res.*, *111*, D12314, doi:10.1029/2005JD006490.

Rodwell, M. J., and B. J. Hoskins (1996), Monsoons and the dynamics of deserts, *Q. J. R. Meteorol. Soc.*, *122*, 1385–1404, doi:10.1002/qj.49712253408.

Rosenlof, K., A. Tuck, K. Kelly, J. Russell III, and M. McCormick (1997), Hemispheric asymmetries in water vapor and inferences about transport in the lower stratosphere, *J. Geophys. Res.*, *102*(D11), 13,213–13,234, doi:10.1029/97JD00873.

Sauvage, B., R. V. Martin, A. van Donkelaar, X. Liu, K. Chance, L. Jaeglé, P. I. Palmer, S. Wu, and T.-M. Fu (2007), Remote sensed and in situ constraints on processes affecting tropical tropospheric ozone, *Atmos. Chem. Phys.*, *7*, 815–838.

Shephard, M. W., et al. (2008), Comparison of Tropospheric Emission Spectrometer (TES) nadir water vapor retrievals with *in situ* measurements, *J. Geophys. Res.*, *113*, D15S24, doi:10.1029/2007JD008822.

Stone, E. M., L. Pan, B. J. Sandor, W. G. Read, and J. W. Waters (2000), Spatial distributions of upper tropospheric water vapor measurements from the UARS Microwave Limb Sounder, *J. Geophys. Res.*, *105*(D10), 12,149–12,161, doi:10.1029/2000JD900125.

Tan, W., M. A. Geller, S. Pawson, and A. M. da Silva (2004), A case study of excessive subtropical transport in the stratosphere of a data assimilation system, *J. Geophys. Res.*, *109*, D11102, doi:10.1029/2003JD004057.

Tangborn, A., I. Stajner, M. Buchwitz, I. Khlystova, S. Pawson, J. Burrows, R. Hudman, and P. Nedelec (2009), Assimilation of SCIAMACHY total column CO observations: Global and regional analysis of data impact, *J. Geophys. Res.*, doi:10.1029/2008JD010781, in press.

von Kuhlmann, R., M. G. Lawrence, P. J. Crutzen, and P. J. Rasch (2003), A model for studies of tropospheric ozone and nonmethane hydrocarbons: Model description and ozone results, *J. Geophys. Res.*, *108*(D9), 4294, doi:10.1029/2002JD002893.

Wang, Y., D. J. Jacob, and J. A. Logan (1998a), Global simulation of tropospheric O_3-NO_x-hydrocarbon chemistry, 3. Origin of tropospheric ozone and effects of non-methane hydrocarbons, *J. Geophys. Res.*, *103*(D9), 10,757–10,768, doi:10.1029/98JD00156.

Wang, Y., J. A. Logan, and D. J. Dacob (1998b), Global simulation of tropospheric O_3-NO_x-hydrocarbon chemistry: 2. Model evaluation and global ozone budget, *J. Geophys. Res.*, *103*(D9), 10,727–10,755, doi:10.1029/98JD00157.

Weaver, C. J., A. R. Douglass, and R. B. Rood (1993), Thermodynamic balance of three-dimensional stratospheric winds derived from a data assimilation procedure, *J. Atmos. Sci.*, *50*, 2987–2993, doi:10.1175/1520-0469(1993)050<2987:TBOTDS>2.0.CO;2.

Wild, O., and H. Akimoto (2001), Intercontinental transport of ozone and its precursors in a three-dimensional global CTM, *J. Geophys. Res.*, *106*(D21), 27,729–27,744, doi:10.1029/2000JD000123.

Worden, J., et al. (2006), Tropospheric Emission Spectrometer observations of the tropospheric HDO/H_2O ratio: Estimation approach and characterization, *J. Geophys. Res.*, *111*, D16309, doi:10.1029/2005JD006606.

Worden, J. R., D. Noone, K. Bowman, and TES Team Members (2007), Importance of rain evaporation and continental convection in the tropical water cycle, *Nature*, *445*, 528–532, doi:10.1038/nature05508.

Yevich, R., and J. A. Logan (2003), An assessment of biofuel use and burning of agricultural waste in the developing world, *Global Biogeochem. Cycles*, *17*(4), 1095, doi:10.1029/2002GB001952.

Yienger, J., M. Galanter, T. Holloway, M. Phadnis, S. Guttikunda, G. Carmichael, W. Moxim, and H. Levy II (2000), The episodic nature of air pollution transport from Asia to North America, *J. Geophys. Res.*, *105*(D22), 26,931–26,945, doi:10.1029/2000JD900309.

Zhang, L., et al. (2006), Ozone-CO correlations determined by the TES satellite instrument in continental outflow regions, *Geophys. Res. Lett.*, *33*, L18804, doi:10.1029/2006GL026399.

Zhou, T.-J., and Z.-X. Li (2002), Simulation of the east Asian summer monsoon using a variable resolution atmospheric GCM, *Clim. Dyn.*, *19*, 167–180, doi:10.1007/s00382-001-0214-8.

Ziemke, J. R., S. Chandra, B. N. Duncan, L. Froidevaux, P. K. Bhartia, P. F. Levelt, and J. W. Waters (2006), Tropospheric ozone determined from Aura OMI and MLS: Evaluation of measurements and comparison with the Global Modeling Initiative's Chemical Transport Model, *J. Geophys. Res.*, *111*, D19303, doi:10.1029/2006JD007089.

Ziv, B., H. Assroni, and P. Alpert (2004), The factors governing the summer regime of the eastern Mediterranean, *Int. J. Climatol.*, *24*, 1859–1871, doi:10.1002/joc.1113.

D. B. A. Jones, J. Kar, J. J. Liu, and M. Parrington, Atmospheric Science, Department of Physics, University of Toronto, 60 St. George Street, Toronto, ON M5S 1A7, Canada. (jliu@atmosp.physics.utoronto.ca)

D. Noone, Department of Atmospheric and Oceanic Sciences, University of Colorado at Boulder, Boulder, CO 80309-0311, USA.

J. R. Worden, Earth and Space Sciences Division, Jet Propulsion Laboratory, California Institute of Technology, 4800 Oak Grove Drive, MS 183-617, Pasadena, CA 91109, USA.